

# A Conserved Lysine in $\beta$ -Lactam Synthetase Assists Ring Cyclization: Implications for Clavam and Carbapenem Biosynthesis

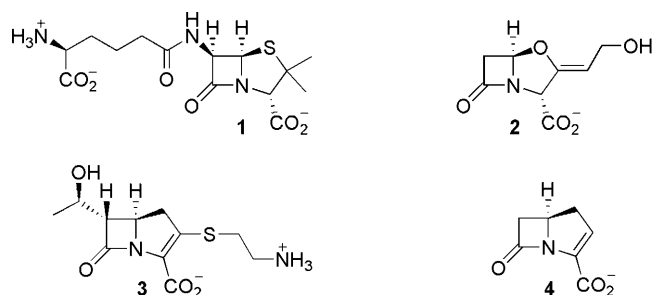
Mary L. Raber,<sup>[a]</sup> Alvaro Castillo,<sup>[b]</sup> Alexander Greer,<sup>\*,[b]</sup> and Craig A. Townsend<sup>\*,[a]</sup>

$\beta$ -Lactam synthetase ( $\beta$ -LS) is the paradigm of a growing class of enzymes that form the critical  $\beta$ -lactam ring in the clavams and carbapenem antibiotics.  $\beta$ -LS catalyzes a two-stage reaction in which  $N^2$ -(2-carboxyethyl)-L-arginine is first adenylated, and then undergoes intramolecular ring closure. It was previously shown that the forward kinetic commitment to  $\beta$ -lactam formation is high, and that the overall rate of reaction is partially limited to a protein conformational change rather than to the chemical step alone of closing the strained ring.  $\beta$ -Lactam formation was evaluated on the basis of X-ray crystal struc-

tures, site-specific mutation, and kinetic and computational studies. The combined evidence clearly points to a reaction coordinate involving the formation of a tetrahedral transition state/intermediate stabilized by a conserved Lys. The combination of substrate preorganization, a well-stabilized transition state and an excellent leaving group facilitates this acyl substitution to account for the strong forward commitment to catalysis and to lower the barrier of four-membered ring formation to the magnitude of a protein conformational change.

## Introduction

How the strained four-membered ring of the  $\beta$ -lactam antibiotics is formed is a central question in their biosyntheses. For penicillin and cephalosporins, which are derived from penicillin, an oxygenase requires ferrous ion and one molecule of dioxygen to remove four hydrogens from a tripeptide precursor to create the bicyclic core of isopenicillin N (Scheme 1, **1**) at a



Scheme 1.  $\beta$ -Lactam-containing natural products.

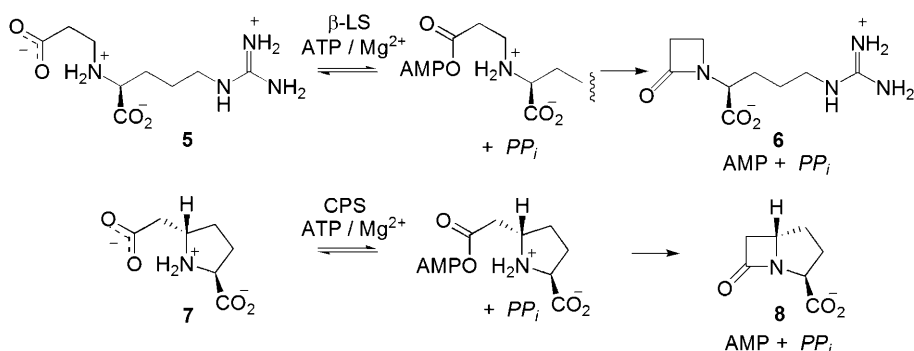
single active site. The considerable strain energy imparted to penicillin during its formation is accounted for thermodynamically in the concomitant reduction of oxygen to two molecules of water for every bicyclic  $\beta$ -lactam formed.<sup>[1]</sup> A mechanistically distinct solution, however, has evolved in the biosynthesis of the potent  $\beta$ -lactamase inhibitor clavulanic acid<sup>[2,3]</sup> (**2**) and the clinically important carbapenem antibiotics, for example, thiamycin<sup>[4,5]</sup> (**3**) and its simplest relative, carbapenem-3-carboxylic acid<sup>[6,7]</sup> (**4**). The first committed step to clavulanic acid is the thiamin-dependent condensation of D-glyceraldehyde-3-phosphate (G3P) and L-arginine to  $N^2$ -(2-carboxyethyl)-arginine<sup>[8–10]</sup> (**5**, CEA). In the critical  $\beta$ -lactam-forming reaction, this

$\beta$ -amino acid is activated with ATP (adenylation) by  $\beta$ -lactam synthetase ( $\beta$ -LS), which then carries out a cyclization reaction to deoxyguanidinoproclavaminc acid (**6**, DGPC) with loss of AMP<sup>[11]</sup> (Scheme 2). A similar process occurs in the biosynthesis of carbapenem-3-carboxylic acid (**4**) during which (2S,5S)-5-carboxymethyl proline (**7**) is transformed to (3S,5S)-carbapen-2-am-3-carboxylate (**8**) by carbapenam synthetase (CPS).<sup>[12]</sup> Here, the energetic cost of  $\beta$ -lactam formation is paid by the hydrolysis of ATP. Against expectation, however, protein conformational changes were discovered to be substantially rate-controlling in these two enzyme-catalyzed reactions rather than solely the chemical step of four-membered ring closure.<sup>[13,14]</sup> In fact, in wild-type  $\beta$ -LS, and presumably CPS by comparison, it was shown that the forward rate of  $\beta$ -lactam formation is so great at high pH that acyl-adenylation is rendered effectively irreversible.<sup>[14]</sup> We were intrigued by this outcome and have turned to computational methods, site-directed mutagenesis, and isotope incorporation experiments to understand the mechanism of  $\beta$ -lactam closure mediated by  $\beta$ -LS, and to illuminate how the energy barrier to this process is lowered in

[a] Dr. M. L. Raber, Dr. C. A. Townsend  
Department of Chemistry, The Johns Hopkins University  
Baltimore, MD 21218 (USA)  
Fax: (+1) 410-261-1233  
E-mail: ctownsend@jhu.edu

[b] A. Castillo, Dr. A. Greer  
Department of Chemistry and Graduate Center and  
The City University of New York (CUNY), Brooklyn College  
Brooklyn, NY 11210 (USA)  
Fax: (+1) 718-951-4607  
E-mail: agreer@brooklyn.cuny.edu

Supporting information for this article is available on the WWW under <http://dx.doi.org/10.1002/cbic.200900389>.



Scheme 2.  $\beta$ -LS and CPS-catalyzed reactions.

the enzyme to be comparable to a protein conformational change.

Steady-state kinetic methods have been applied to  $\beta$ -LS to show that an ordered Bi-Ter mechanism takes place in which ATP is the first substrate of two to bind, and pyrophosphate is the last of three products to dissociate after DGPC formation.<sup>[11]</sup> A series of crystallographic snapshots has been obtained at key points in the reaction coordinate. In addition to structures of 1) the resting enzyme and 2)  $\beta$ -LS-ATP, 3) a ternary complex of  $\beta$ -LS, CEA and the nonreactive analogue of ATP, AMP-CPP ( $\beta$ -LS-CEA-AMP-CPP) was obtained. The latter revealed a high degree of substrate preorganization for in-line attack of the CEA carboxylate on ATP, and a favorable *gauche* binding geometry of the substrate for  $\beta$ -lactam formation.<sup>[15,16]</sup> 4) The lower homologue of CEA, carboxymethyl-L-arginine (CMA) fortuitously underwent reaction with ATP in the crystal to reveal the adenylated intermediate and  $PP_i$  coordinated to two  $Mg^{2+}$  ions. 5) Finally, a fifth structure was obtained with  $\beta$ -LS bound to all three products DGPC,  $PP_i$  and AMP.<sup>[15]</sup> In these structures there is a disordered loop (residues 444–453), which becomes organized over the active site when it contains the adenylated intermediate or the final products. A tyrosyl-glutamyl catalytic dyad visible in these X-ray snapshots has been shown to deprotonate the secondary amine of the  $\beta$ -amino acid substrate of not only  $\beta$ -LS but also CPS to initiate cyclization of the four-membered rings.<sup>[17]</sup> Moreover, two additional residues potentially important for the chemical step of  $\beta$ -lactam formation were apparent in the  $\beta$ -LS structures. At the N terminus of the mobile loop lies Lys443, the  $\epsilon$ -nitrogen of which is in close proximity to the carbonyl of the adenylated CMA ( $N^\epsilon-O=3.5 \text{ \AA}$ ) and the product, DGPC ( $N^\epsilon-O=3.0 \text{ \AA}$ ). The second, His447, is located on the catalytic loop, and its  $\pi$ -nitrogen is near the carboxymethyl side chain C1 of the adenylated CMA intermediate suggesting its possible role as a catalytic base.

Studies of the mechanism of acyl substitution reactions are well-developed in the literature.<sup>[18–22]</sup> We wished to consider all possible routes that could account for the low-energy path acting in enzyme-catalyzed  $\beta$ -lactam formation. For highly reactive acyl groups, for example, acyl halides, or, by analogy, acyl-adenylates in the present instance, elimination to a ketene is a possible reaction path (Scheme 3, path A).<sup>[23,24]</sup> The efficient intramolecular attack of a secondary amine onto a ketene in

this manner has been exemplified in a close precedent.<sup>[25]</sup> In the X-ray structure of  $\beta$ -LS-CMA-AMP- $PP_i$  a distance of 4.7  $\text{\AA}$  can be measured from the histidine nitrogen to the  $\alpha$ -carbon of the activated carboxymethyl side chain. The distance to this methylene hydrogen will be greater than, and therefore will overestimate, the actual distance to the ethylene hydrogen of the native  $\beta$ -LS substrate, CEA (5), which contains an additional methylene. The crystal structure of  $\beta$ -LS and the final products showed the relevant histidine nitrogen further from the  $\alpha$ -carbon of the  $\beta$ -lactam ring in DGPC (6; 5.6  $\text{\AA}$ ). The placement of His447 prior to  $\beta$ -lactam formation suggests that this active site base could be well-positioned to catalyze such an elimination process. Moreover, in-plane attack by the  $\beta$ -nitrogen in CEA can be visualized to be geometrically attainable on the  $sp$ -hybridized central carbon of the hypothetical ketene intermediate for  $\beta$ -lactam formation.

Alternatively, a highly reactive acyl intermediate could ionize directly to an acylium ion (Scheme 3, path B).<sup>[26–28]</sup> Like a ketene, this highly electrophilic species would similarly present an in-plane orbital arrangement for cyclization. It is known in the acid-catalyzed hydrolysis of  $\beta$ -lactams that  $N$ -protonation leads to the reversible scission of the lactam bond, which results in a secondary amine and an acylium ion. To complete the overall hydrolysis reaction, water then adds to the acylium intermediate.<sup>[29,30]</sup> In the present instance, however, ionization of the intermediate acyl-adenylate would give the acylium ion in the presence of a secondary amine. These species would lead to the formation of the protonated  $\beta$ -lactam but in the added presence of AMP dianion, which would rapidly deprotonate the  $N$ -protonated  $\beta$ -lactam ( $pK_a=0$  to  $-3$ <sup>[30]</sup>) driving the equilibrium in the direction of ring closure, the microscopic reverse of this step in hydrolysis.

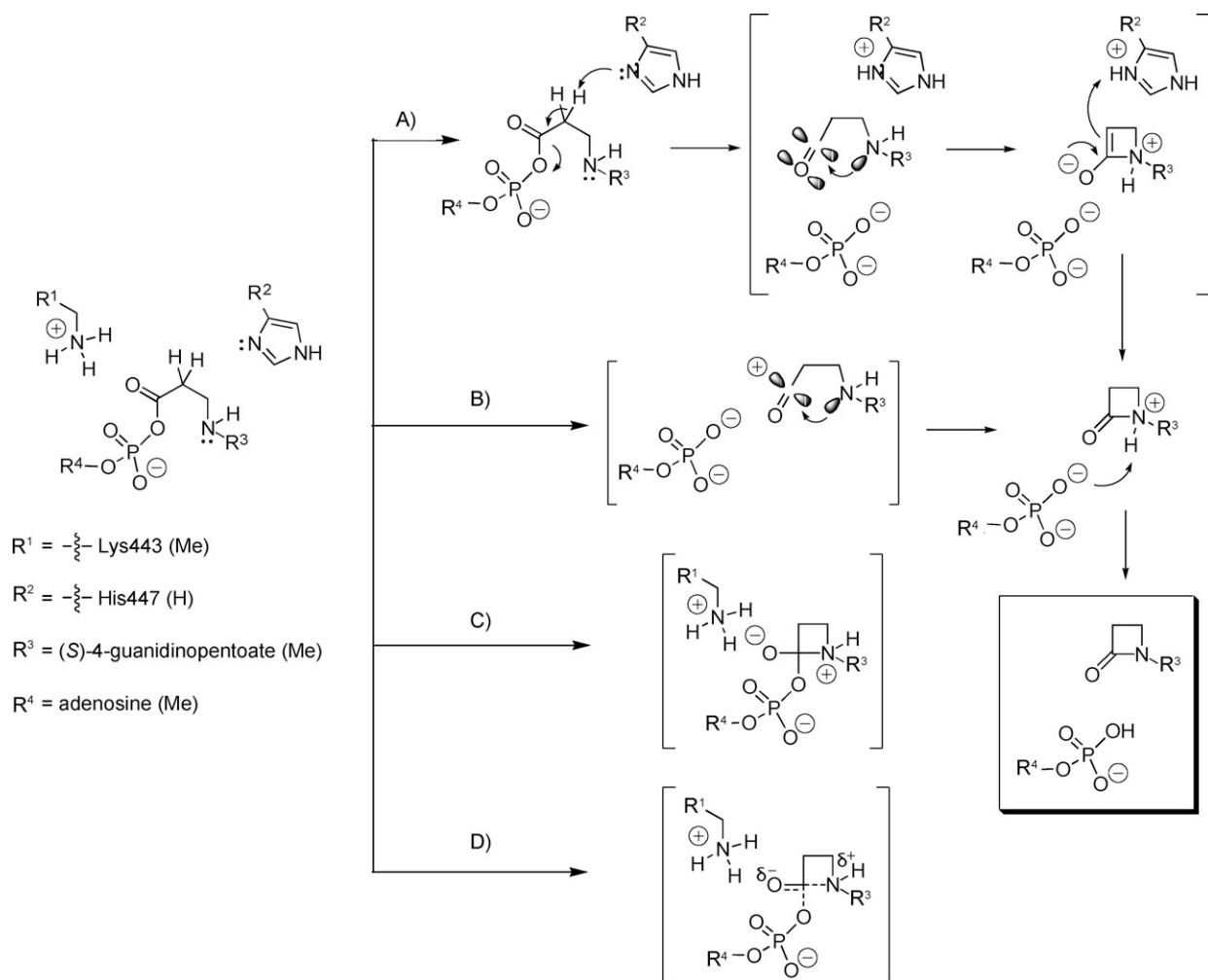
More conventional routes to  $\beta$ -lactam formation would invoke nitrogen addition to the acyl-adenylate and the transient formation of a tetrahedral intermediate (Scheme 3, path C) followed by AMP loss, or a more concerted process involving only a tetrahedral transition state (Scheme 3, path D). From the X-ray structures it can be hypothesized that Lys443 could stabilize the formation of such a tetrahedral transition state or intermediate by hydrogen bonding or proton donation to the carbonyl oxygen.

More conventional routes to  $\beta$ -lactam formation would invoke nitrogen addition to the acyl-adenylate and the transient formation of a tetrahedral intermediate (Scheme 3, path C) followed by AMP loss, or a more concerted process involving only a tetrahedral transition state (Scheme 3, path D). From the X-ray structures it can be hypothesized that Lys443 could stabilize the formation of such a tetrahedral transition state or intermediate by hydrogen bonding or proton donation to the carbonyl oxygen.

## Results and Discussion

### Consideration of a ketene and acylium ion intermediates

To probe the possible involvement of a ketene mechanism (path A), a deuterium-incorporation experiment was carried out. Recombinant  $\beta$ -LS was diluted approximately tenfold in 99.9%  $D_2O$  and used to initiate synthesis in a preincubated



**Scheme 3.** Four proposed mechanisms (A–D) from the acyl-adenylate intermediate to  $\beta$ -lactam formation in  $\beta$ -LS. R represents the functional groups found in vivo, while the groups shown in parentheses represent those used in DFT calculations.

assay mixture containing ATP/Mg<sup>2+</sup>, DTT, and CEA at pD 7.8. These assay components were exchanged in 99.9% D<sub>2</sub>O and lyophilized three times prior to the addition of enzyme to ensure >95% deuterium in the reaction mixture. Previous solvent isotope effect experiments ensured that the active site of  $\beta$ -LS is accessible for isotopic exchange.<sup>[17]</sup> As a control, a reaction in 100% H<sub>2</sub>O (pH 7.8) was performed in parallel. ESI-MS analysis from isolated DGPC in both reactions gave clear parent ions (*m/z* 229) accompanied by indistinguishable isotopic clusters indicating no incorporation of deuterium during  $\beta$ -lactam formation.

A pH versus  $\log k_{\text{cat}}$  profile of  $\beta$ -LS revealed catalysis to be dependent on the deprotonation of an ionizable group with a  $pK_{\text{a}}$  of 8.1.<sup>[14]</sup> To further test if His447 is a catalytic base and responsible for the observed  $pK_{\text{a}}$  in the wild-type enzyme, this residue was mutated to alanine. The mutant remained catalytically active showing a 20-fold decrease in  $k_{\text{cat}}$ . The kinetic data were fitted to Equation (1):

$$\log k_{\text{cat}} = \log \left[ \frac{(x)_{\text{max}} + (x)_{\text{min}} \times 10^{\text{pH} - \text{p}K_{\text{a}}1}}{1 + 10^{\text{pH} - \text{p}K_{\text{a}}1}} \right] \quad (1)$$

where  $(x)_{\text{max}}$  and  $(x)_{\text{min}}$  correspond to the upper or lower limits of the linear fit, respectively, to give a  $pK_{\text{a}}$   $7.9 \pm 0.2$  in a  $\text{pH}-k_{\text{cat}}$  profile (Figure 1)—a value virtually identical to that of the general base revealed in the wild-type enzyme. His447 is, there-

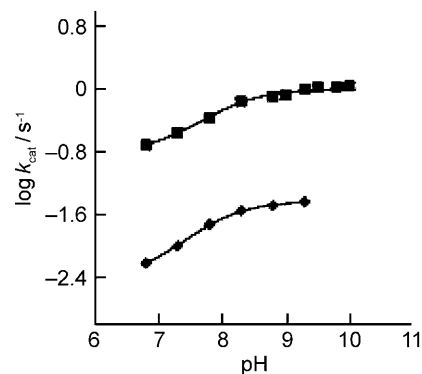


**Figure 1.** The pH versus  $\log k_{\text{cat}}$  profiles at 25 °C of wild-type  $\beta$ -LS (ref. [14]; ■) and His447Ala (▲). Error bars are shown for all data points and do not exceed the size of the data points when not visible.

fore, not a catalytic base and, combined with the absence of deuterium uptake into the product, the possible intermediacy of a ketene in the  $\beta$ -lactam closure step can be excluded.

The four potential reaction pathways depicted in Scheme 3 were also evaluated by DFT methods (see below and the Supporting Information). The ketene (path A) and acylium (path B) mechanisms were both found to be high-energy alternatives for  $\beta$ -lactam formation and, in accord with the biochemical results above, could be removed from further consideration.

### Lysine-assisted $\beta$ -lactam formation

The placement of Lys443 in  $\beta$ -LS crystal structures suggested its importance in  $\beta$ -lactam formation. While its mutation to alanine and methionine in CPS afforded no detectable activity,<sup>[13]</sup> in vitro kinetic assays of the Lys443Arg  $\beta$ -LS mutant at the wild-type pH optimum showed a large drop in  $k_{\text{cat}}$  along with a diminished forward commitment to catalysis after acyl-adenylation.<sup>[14]</sup>

In the present study, upon pH variation with the Lys443Arg mutant, it became clear that the pH optimum of this mutant had shifted significantly higher than that of wild-type  $\beta$ -LS and lay above the experimental limit of the buffer system (pH 10.5). While the change in the  $k_{\text{cat}}$  of Lys443Arg relative to that of the wild type optimal activity ( $1.1 \text{ s}^{-1}$ ) is 1400-fold lower at pH 7.8, this ratio shrinks to 80-fold at pH 10.5; this illustrates that factors governing DGPC formation become significantly more favorable in the Lys443Arg mutant as pH is increased (Table 1). From the kinetic parameters it was also clear that the  $K_{\text{M,CEA}}$  of this mutant steadily increased from  $120 \mu\text{M}$  at pH 7.8 to  $950 \mu\text{M}$  at pH 10.5, which implies that the protonated form of Lys443 is more favorable for substrate capture, presumably owing to substrate charge stabilization as suggested previously in the X-ray structural analysis.<sup>[15]</sup>

The pH dependence of enzyme kinetic parameters reveals ionizable group(s) important for catalysis, binding, and enzyme conformation. While the pH- $(k_{\text{cat}}/K_{\text{M}})$  profile is relatively pH independent (slope=0.17) and could represent numerous groups contributing to substrate capture in the Lys443Arg

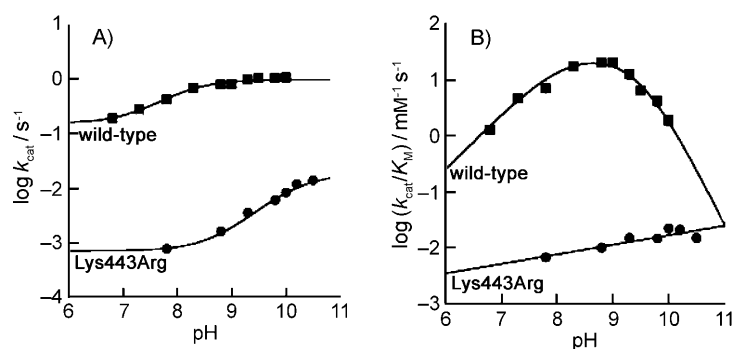


**Figure 2.** The pH-rate profiles of Lys443Arg mutant. A) The pH versus  $\log k_{\text{cat}}$ , and B)  $k_{\text{cat}}/K_{\text{M}}$  profiles at  $25^\circ\text{C}$  of wild-type  $\beta$ -LS (see ref. [14]) and Lys443Arg. Error bars are shown for all data points and do not exceed the size of the data points when not visible.

mutant, the pH versus  $\log k_{\text{cat}}$  profile is affected by group(s) that influence catalysis (Figure 2). The Lys443Arg pH- $\log k_{\text{cat}}$  profile was best fit to Equation (1) with an  $R^2$  of 0.996, from which was calculated a single  $\text{p}K_{\text{a}}$  of  $10.13 \pm 0.06$ . This value was two  $\text{p}K_{\text{a}}$  units higher than that of wild type ( $\text{p}K_{\text{a}}=8.1$ ). The significantly increased  $\text{p}K_{\text{a}}$  is consistent with the newly introduced arginine residue being titrated, rather than the original lysine. In water, a lysine residue ( $\text{p}K_{\text{a}}=10.5$ ) is predicted to have a  $\text{p}K_{\text{a}}$  two units lower than that of arginine ( $\text{p}K_{\text{a}}=12.5$ ). While a  $\text{p}K_{\text{a}}$  of 8.1 is lower than the reference value of 10.5 in water, the  $\text{p}K_{\text{a}}$  values of residues in enzyme active sites typically vary from their standard values owing to a lower dielectric environment in the protein interior.<sup>[31,32]</sup> This will cause the  $\text{p}K_{\text{a}}$  values of bases to be lower than expected. In the case of  $\beta$ -LS, the catalytic loop shields the active site from the surrounding aqueous medium during catalysis and a perturbation in  $\text{p}K_{\text{a}}$  would be expected. Together, these considerations support Lys443 as the ionizable group the deprotonation of which is essential to  $\beta$ -LS catalysis with the observed change in  $\text{p}K_{\text{a}}$  consistent with the substitution of arginine for lysine at this position. The ability of arginine to act as a base in enzymatic reactions is preceded in several other systems.<sup>[33]</sup>

To account for the behavior of the pH- $k_{\text{cat}}$  profile in  $\beta$ -LS, it is possible that the  $\beta$ -LS mechanism is similar to an isomechanism,<sup>[34]</sup> as previously suggested.<sup>[14]</sup> In this way, proton assistance by Lys443 would occur during  $\beta$ -lactam ring closure and

its charge rebound or reprotonation is coupled to its rate-determining conformational change (i.e., relaxation of the active-site loop).<sup>[14]</sup> This sort of active site "recharging" is preceded in kinetic studies of aspartyl proteases<sup>[35–37]</sup> and triose-phosphate isomerase.<sup>[38,39]</sup> Perhaps the mutation of Lys443 to a residue with a higher  $\text{p}K_{\text{a}}$  (i.e., arginine) disrupts this loop relaxation, causing four-membered ring formation to now be fully rate determining. Since vis-

**Table 1.** Comparison of pH-dependent kinetic parameters<sup>[a]</sup> of  $\beta$ -LS and mutant Lys443Arg.

pH	Wild-type $k_{\text{cat}}$ [ $\text{s}^{-1}$ ]	Lys443Arg $k_{\text{cat}}$ [ $\text{s}^{-1}$ ]	Wild-type $K_{\text{M,CEA}}$ [mM]	Lys443Arg $K_{\text{M,CEA}}$ [mM]	Fold change $^{-}\Delta k_{\text{cat}} + \Delta K_{\text{M}}$
7.8	$0.43 \pm 0.01$	$0.00079 \pm 0.00001$	$0.057 \pm 0.007$	$0.12 \pm 0.01$	540 2
8.8 <sup>[a]</sup>	$0.82 \pm 0.01$	$0.0016 \pm 0.0001$	$0.044 \pm 0.002$	$0.19 \pm 0.02$	510 4
9.3 <sup>[a]</sup>	$1.01 \pm 0.03$	$0.0036 \pm 0.0001$	$0.082 \pm 0.007$	$0.24 \pm 0.02$	280 3
9.8	$1.08 \pm 0.03$	$0.00615 \pm 0.00004$	$0.26 \pm 0.02$	$0.40 \pm 0.01$	170 1.5
10.0	$1.09 \pm 0.05$	$0.0083 \pm 0.0002$	$0.57 \pm 0.06$	$0.37 \pm 0.02$	130 1.5 <sup>[b]</sup>
10.2	n.a.	$0.0120 \pm 0.0003$	n.a.	$0.57 \pm 0.05$	n.a. n.a.
10.5	n.a.	$0.0140 \pm 0.0004$	n.a.	$0.95 \pm 0.07$	n.a. n.a.

[a] Wild-type parameters at all pH values and mutant parameters at pH 8.8 and 9.3 are from previously published kinetic data (ref. [14]). [b] Value reflects a fold decrease in  $K_{\text{M,CEA}}$  of Lys443Arg relative to wild type. Approximate fold decreases or increases are shown as  $^{-}\Delta$  or  $^{+}\Delta$ , respectively, with wild-type kinetic values divided by mutant kinetic parameters to give the values shown; n.a.: not applicable.

cosity variation at pH 9.3<sup>[14]</sup> and 10.4 (see the Supporting Information) had no significant effect on the  $k_{\text{cat}}$ , it ensured that the chemical step alone is rate-determining throughout the relevant pH range for this mutant and not a viscosity-dependent conformational change.<sup>[40]</sup> This observation is unlike the large viscosity dependence determined for wild type at basic pH values.<sup>[14]</sup>

In accord with these kinetic measurements, the catalytic role of Lys443 can be visualized in the crystal structures of the  $\beta$ -LS active site. This series of static images illustrates that prior to chemistry, Lys443 is in closer proximity to the oxygen of the  $\alpha$ -phosphate in AMP-CPP than to the carboxylate awaiting adenylation. After reaction with ATP, the Lys443 primary amine is then 3.5 Å away from the activated carbonyl oxygen of the acyl-adenylate.<sup>[15]</sup> In X-ray snapshots of the  $\beta$ -LS-DGPC-AMP-PP<sub>i</sub> complex, this nitrogen moves even closer to the  $\beta$ -lactam oxygen.<sup>[15]</sup>

### Computational analysis of $\beta$ -lactam formation

Computational methods were guided by the X-ray data and allowed the prediction of geometries and high-energy intermediates, which were not obtainable from experimental methods alone. Since density functional theory (DFT) has been commonly used to answer questions related to  $\beta$ -lactams, we turned to this type of theoretical analysis to evaluate the role of Lys443 in DGPC formation using the model 4-(methylamino)butan-2-one-1-(methyl)-hydrogenphosphate (**9**, Figure 3) to represent the acyl-adenylate of CEA. The adenylated-CEA model bears similarity to CEA (**5**), but with a truncated structure for ease of computation. Since the arginine side chain of CEA and the adenosine of AMP are constrained in all collected  $\beta$ -LS crystal structures and do not participate in the catalytic chemistry, these moieties were abbreviated in the CEA model.

$\beta$ -LS-CMA-AMP-PP<sub>i</sub> and  $\beta$ -LS-DGPC-AMP-PP<sub>i</sub> structures revealed that Lys-N<sup>ε</sup>-O1 distances were in the range of 3–4 Å. Using these observations, the potential energy surface was

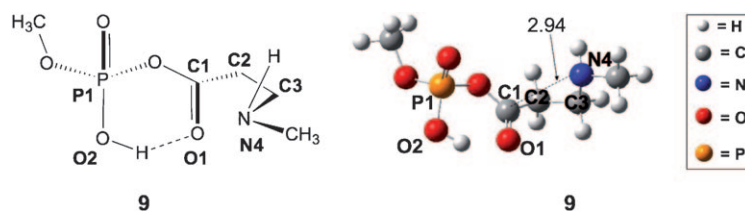


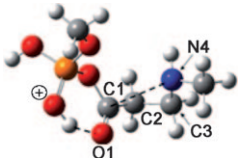
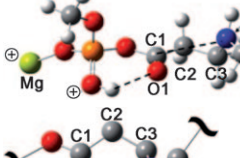

Figure 3. ChemDraw (left) and GaussView (right) generated structures for **9** (bond distance is in Å).

computed, which considered an accurately positioned lysine relative to **9**. The donation of a lysyl proton to the model showed that this event was accompanied by a reduction of electron density at O1 and O2 as revealed by natural bond order (NBO) charges. The reduced negative charge suggests that proton assistance from lysine is not dominated by electrostatics, but rather by proton transfer. For example, the NBO charge<sup>[41]</sup> on O1 of the CEA model prior to proton transfer (−0.64) is reduced compared to its corresponding charge (−0.55) after this event (see the Supporting Information). Compound **10** represents the resulting complex that contains the interacting proton donated from lysine (see the Supporting Information).

Since Mg<sup>2+</sup> is thought to aid in stabilizing the phosphate negative charge of the adenylated CEA in  $\beta$ -LS, a control for **10** was studied (**10b**), which replaced the proton on the oxyanion of P1 that was originally used to stabilize this negative charge in the calculations. The similar values in Table 2 imply that model **10** is qualitatively reasonable with respect to **10b**. Moreover, the energetics involved in the initial step from **10** and **10b** leading to a  $\beta$ -lactam are comparable and within 1–4 kcal mol<sup>−1</sup> as determined by the B3LYP calculations by using the 6-31G(d) basis set and the 6-311+G(d,p) basis set with diffuse functions (see the Supporting Information).

The data in Table 2 also show that the B3LYP/6-31G(d) level describes well the *gauche* conformation as illustrated in **10**. The **10** and **10b** structures were compared to the X-ray crystal

Table 2. Calculated and experimental values of truncated CEA structural parameters.<sup>[a]</sup>

Compound	Bond distance [Å]			Bond angle [degrees]		Dihedral angle [degrees]
	C1–O1	C1–N4	C1–C2	O1–C1–C2	C1–C2–C3	C1–C2–C3–N4
 <b>10</b>	1.20	2.71	1.50	128.5	106.6	−49.8
 <b>10b</b>	1.20	3.09	1.50	129.1	112.7	−69.4
 CEA crystal structure	(1.26)	(3.03)	(1.54)	(118.7)	(114.0)	(−53.9)

[a] Experimental values are in parentheses.

data of the preorganized CEA, which is positioned for in-line attack on the  $\alpha$ -phosphorus of the ATP analogue, AMP-CPP.<sup>[26]</sup> The *gauche* conformation is best shown when comparing the calculated C1–C2–C3–N4 dihedral angle of **10** ( $-49.8^\circ$ ) and **10b** ( $-69.4^\circ$ ), which are similar to the X-ray value ( $-53.9^\circ$ ). While the calculated O1–C1–C2 bond angles in **10** ( $128.5^\circ$ ) and **10b** ( $129.1^\circ$ ) are slightly overestimated compared to that of the CEA crystal structure ( $118.7^\circ$ ) the bond distances match well the preorganization of CEA observed in the X-ray data.

The binding of CEA in the *gauche* conformation in the  $\beta$ -LS active site reduces a significant energetic cost compared to its *anti* form. DFT calculations estimated that this high-energy conformer of CEA is about  $24 \text{ kcal mol}^{-1}$  less stable than the corresponding *anti* form. The large energy difference suggests that this conformational modification imparted by  $\beta$ -LS acts in concert with Lys443 to reduce the energetic barrier to  $\beta$ -lactam formation.

The potential energy surface from **10** to the monocyclic  $\beta$ -lactam shown in **13** was computed and is illustrated in Figure 4. The DFT-calculated energy profile agrees with the experimental evidence, in which  $\beta$ -lactam formation in  $\beta$ -LS is not a high-energy process, but rather an overall exothermic course is followed from **10** to **13**; a similar energetic profile was also computed when considering solvent effects. The computational findings point to the importance of paths C and D in Scheme 3, with an interacting proton assisting in the formation of the  $\beta$ -lactam product (Figure 4). More specifically the potential energy surface infers that  $\beta$ -LS most likely utilizes path D, since the tetrahedral intermediate **12** resides in a very shallow potential well ( $< 0.5 \text{ kcal mol}^{-1}$ ) and rapidly converts to  $\beta$ -lactam **13**. It was not possible to locate a low-energy pathway for  $\beta$ -lactam formation in the absence of lysyl proton assistance. This landscape also revealed that the interacting proton initially resides on O2, since the extent to which the proton is transferred is greater at P1=O2 than carbonyl C1=O1.

However, an energetically low-lying process is computed from **10** to **11** representing an intramolecular proton transfer from O2 to O1 with an activation barrier of  $4 \text{ kcal mol}^{-1}$ .

### Conservation of the catalytic lysine in $\beta$ -lactam synthetases

Clavulanic acid, (5*R*)-carbapen-3-em carboxylate, and thienamycin biosyntheses constitute pathways distinct from that of the well-studied penicillin/cephalosporins.<sup>[42,43]</sup> The sequence homology among these  $\beta$ -lactam-closing enzymes suggests that these ATP-driven steps share common mechanistic features. The genes *bls2* and *thnM* encode the  $\beta$ -lactam synthetases in clavulanic acid and thienamycin biosyntheses, respectively. Both *carA* and *cpmA* genes encode the  $\beta$ -lactam-synthesizing enzymes in the formation of (5*R*)-carbapen-3-em carboxylate.<sup>[7,44]</sup> Interestingly, the gene cluster of the monocyclic  $\beta$ -lactam tabtoxin harbors *tblS* (*orf10*)—the corresponding protein of which also has sequence homology to  $\beta$ -LS (BlS2; 24% identity, 42% similarity).<sup>[45]</sup>

From multiple-sequence alignments of the  $\beta$ -lactam synthetases in clavam, carbapenem, and tabtoxin biosynthesis it is evident that the catalytic lysine (Lys443 in  $\beta$ -LS) is strictly conserved (Figure 5). The data suggest that the role of Lys443 in stabilizing the transition state of  $\beta$ -lactam formation in  $\beta$ -LS is similarly retained among all of its homologues, and this point is underscored by mutagenesis studies of Lys443 in CPS<sup>[13]</sup> and  $\beta$ -LS.<sup>[14]</sup>

Moreover, it is noteworthy that Lys443 lies immediately before the catalytic loop in  $\beta$ -LS (residues 444–453), and is part of the corresponding loop in CPS. Hence, the protonation state of the conserved lysine could influence the interconversion of the open and closed forms of this active-site feature. In addition to structural evidence from  $\beta$ -LS and CPS, primary-sequence alignments suggest that this loop is also conserved in their homologues CpmA and ThnM (Figure 5).

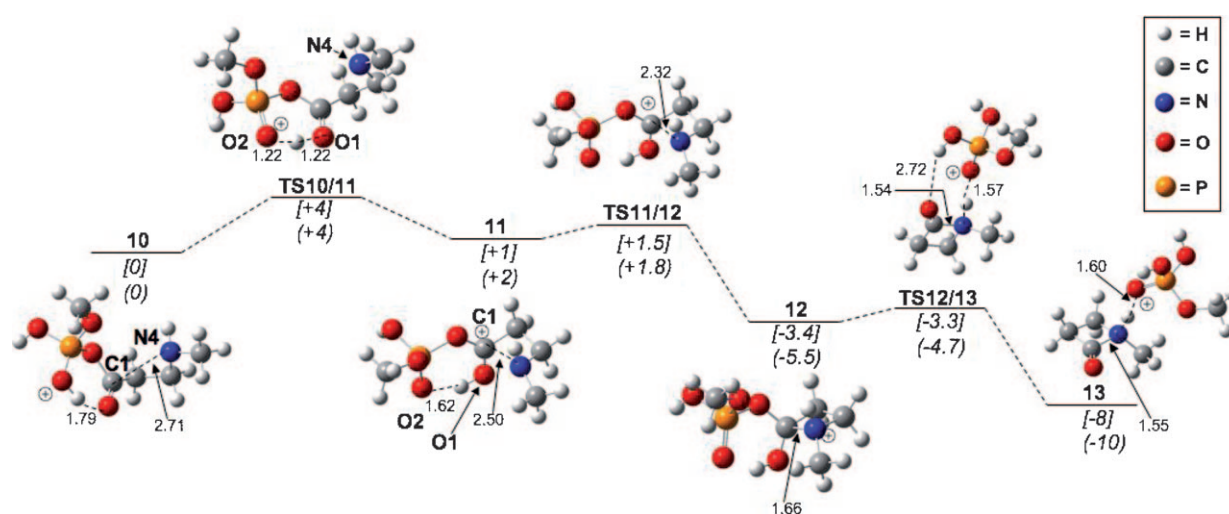


**Figure 4.** B3LYP/6-31G(d) and PCM//B3LYP/6-31G(d) calculated potential energy surface for the conversion of intermediate **12** to  $\beta$ -lactam **13**. The plotted diagram represents the relative energies calculated by using B3LYP/6-31G(d). Gas-phase energies are in brackets, aqueous-phase energies are in parentheses, bond distances are in Å, and energies are in  $\text{kcal mol}^{-1}$ .



**Figure 5.** Truncated sequence alignment of  $\beta$ -lactam synthetases. The red circle shows Lys443 and the dashed line highlights the catalytic loop in  $\beta$ -LS. Dark blue to light blue shows identical sequence to modest sequence similarity, respectively.

## Conclusions

Site-specific mutation, pH, kinetic and computational studies implicate Lys443 in the activation of  $N^2$ -(2-carboxyethyl)-arginine (**5**, CEA) to facilitate formation of the  $\beta$ -lactam deoxyguanidinoproclavaminc acid (**6**, DGPC). Isotope incorporation and kinetics experiments exclude ketene or acylium intermediates (Scheme 3, paths A and B). Simulations of these chemically predated but high-energy pathways served as controls for the DFT methods employed in this paper, which identified a significantly lower energy process in which intramolecular acyl substitution of the adenylated CEA by the substrate  $\beta$ -nitrogen is catalyzed by  $\beta$ -LS (Scheme 3, path D). Proton donation by the conserved active site Lys443 stabilizes the tetrahedral transition state to substantially lower the barrier of this chemical step and facilitate the large forward commitment to  $\beta$ -lactam formation.

Primary-sequence comparisons and X-ray data suggest that this catalytic strategy is general among the members of this family of  $\beta$ -lactam-synthesizing enzymes. While ATP activation affords an excellent leaving group, substrate preorganization, participation of a catalytic dyad, and key transition state stabilization by Lys443 act in a coordinated fashion to lower the barrier of  $\beta$ -lactam cyclization to become energetically comparable to that of a conformational change involving an active-site loop to allow product release.

## Experimental Section

**Materials:** Most assay components and buffers were purchased from Sigma Chemical, Co. (St. Louis, MO, USA).  $D_2O$  was purchased from Cambridge Isotope Laboratories (Andover, MA, USA). CEA and DGPC were synthesized as described previously.<sup>[14,46]</sup>

**Construction, overproduction, and purification of  $\beta$ -LS mutants:** Overlap extension was used to introduce desired  $\beta$ -LS mutations in PCR amplifications with appropriate PCR primers for His447Ala (Table S1 in the Supporting Information). The pET29b/Lys443Arg construct along with overproduction and purification techniques are described elsewhere.<sup>[14]</sup>

**Steady-state continuous assays:** Initial velocities were measured by using a coupled-enzyme assay that quantitates the formation of AMP, as previously used with  $\beta$ -LS,<sup>[14]</sup> with a Cary 50 UV/Vis spectrophotometer at 25 °C. In addition, DGPC formation was confirmed for His447Ala and Lys443Arg through HPLC analysis with an authentic DGPC standard by using previously published protocols.<sup>[11]</sup> The second substrate to bind, CEA, was the varied substrate in all experiments with ATP held constant at saturating levels (2 mM CEA). All assays were conducted in duplicate.

The pH dependence of Lys443Arg was measured by varying CEA from 50  $\mu$ M to 3 mM, while His447Ala was analyzed by using saturated CEA concentrations of 2 mM ( $\sim 20 \times K_{M,CEA}$  at pH 7.8) with the three-buffer systems previously described.<sup>[14]</sup> Profiles were plotted as the  $\log k_{cat}$  or  $\log(k_{cat}/K_M)$  as a function of pH. The  $k_{cat}$  parameters were analyzed with a nonlinear

fit [Eq. 1] while the Lys443Arg  $k_{cat}/K_M$  parameters showed linear dependence. Mutants were stable in the entire pH range reported, evidenced by measuring their activity after incubation at the appropriate pH for at least the length of the assays. The error bars shown were propagated from the uncertainty on each rate to a natural logarithmic function.

Viscosity dependence was analyzed at pH 10.4 with CEA varied from 50  $\mu$ M to 4 mM. Assays were performed with the microviscogen glycerol (0–30%, w/v) and the viscosities of the solutions were determined in triplicate by using a Brookfield viscometer. The errors shown in the plots were propagated in quadrature from the fractional uncertainties of the respective rates (see the Supporting Information).

**Deuterium incorporation:** In the  $\beta$ -LS-catalyzed reaction, possible deuterium incorporation at the  $\alpha$ -carbon of  $\beta$ -lactam DGPC was analyzed in a reaction containing >95%  $D_2O$ .

1) *Deuterium incorporation assay:* Reactions were run in parallel at 100%  $H_2O$  and >95%  $D_2O$  at room temperature in Tris (80 mM, pH 7.8),  $MgCl_2$  (13 mM), ATP (0.7 mM), CEA (2 mM), and  $\beta$ -LS (0.9  $\mu$ M) for 2.25 h in a final volume of 1.5 mL. All assay components prior to the  $D_2O$  reaction were dissolved in  $D_2O$ , flash frozen with liquid nitrogen, and lyophilized to dryness. This series of exchange steps was repeated three times with the pH adjusted by using DCl prior to the assay. Reactions were quenched by heating to 100 °C for 2 min and centrifuged to remove precipitated protein. The supernatant was flash frozen with liquid nitrogen in 100–200  $\mu$ L aliquots and stored at  $-20$  °C for later HPLC analysis.

2) *HPLC separation and collection:* In order to isolate DGPC from the reaction mixture, separation was performed by an HPLC isocratic method (100%  $H_2O$ ) by using a Phenomenex Partisil Semi-prep C18 column (9.4  $\times$  250 mm) at  $\lambda = 210$  nm. At 4.3 mL  $min^{-1}$ , DGPC was collected at about 8 min and flash frozen, lyophilized to dryness, and stored at  $-20$  °C until ESI-MS analysis. The elution time was confirmed with an authentic standard.

3) *ESI-MS analysis:* The molecular weights of DGPC collected from reactions performed in  $D_2O$  and  $H_2O$  were compared by using ESI-MS. ESI spectra were acquired in the positive ion mode on a Finnigan LCQ<sup>Deca</sup> ion trap mass spectrometer with an electrospray ion source (ESI) by using a spray voltage of 5.01 kV and capillary temperature of 251.9 °C. Lyophilized samples were dissolved in 1:1  $dH_2O$ /methanol with 1% formic acid immediately prior to direct injection into the ESI chamber by using a syringe pump at a flow rate of 10  $\mu$ L  $min^{-1}$ . Each spectrum was an average of 30 scans. Expected DGPC parent peaks:  $m/z$  229.26 [ $M+H$ ] and 230.26 [ $M+D$ ].

**Steady-state kinetic analysis:** All kinetic data were fit by using Kaleidograph 4.0. Initial velocity patterns were fit to Equation (2) with A representing CEA.

$$v/[E_o] = (k_{cat}A)/(K_M + A) \quad (2)$$

**Theoretical methods:** DFT calculations were performed with the use of the Gaussian 03 program package.<sup>[47]</sup> Geometry optimizations, vibrational frequencies, and intrinsic reaction coordinates (IRCs) were conducted by using DFT with the exchange correlation of B3LYP along with the Pople basis set 6-31G(d).<sup>[48–50]</sup> The B3LYP functional is not without deficiencies;<sup>[51–53]</sup> for example, barrier heights can be underestimated by 4–5 kcal mol<sup>-1</sup> based on a database analysis of 76 diverse barrier heights, which is due to a self interaction error in local DFT.<sup>[54,55]</sup> The average errors of B3LYP in thermochemistry calculations are ~3.6 kcal mol<sup>-1</sup> (from a database of 177 reactions).<sup>[55]</sup> Nonetheless, DFT calculations have been successfully applied to  $\beta$ -lactam systems for predicting structures and conformations, and energetics of reactions, such as ring-opening and decarboxylation.<sup>[56–63]</sup> The DFT calculations reproduce the *gauche* conformation relevant in the crystal data of ( $\beta$ -LS-CEA-AMP-PPP; PDB ID: 1JGT). A proton is used to replace magnesium present in  $\beta$ -LS crystal structures, which stabilizes its negative charge in the active site of  $\beta$ -LS. Comparison of this model to one with magnesium showed a similar energetic pathway to  $\beta$ -lactam formation (see the Supporting Information). While the substrate resides in a protein environment that is not expected to be similar to bulk aqueous solution, from ordering of an active site loop,<sup>[15]</sup> solvent effects were also calculated with the polarized continuum model (PCM) and self-consistent reaction field (SCRF) single point calculations at the B3LYP/6-31G(d) level. The compounds optimize to minima or maxima on the potential energy surface. Molecular structures were viewed with the GaussView program.<sup>[64]</sup>

## Acknowledgements

M.L.R. and C.A.T. thank the NIH (AI014937) for financial support. A.G. thanks the NIH (S06 GM076168-01) and the PSC-CUNY Grants Program for research funding. Computational support was provided by the Graduate Center computational facility and the City University of New York's High Performance Computing Research Center. We thank Dr. Florian Lengyel (CUNY) for assistance with the computational facility and Dr. Michael F. Freeman (JHU) for the pET29b/His447Ala construct and Dr. Fumitaka Kudo (Tokyo Institute of Technology) for early experiments on  $\beta$ -LS.

**Keywords:** beta-lactam • biosynthesis • clavulanic acid • density functional theory • pH-rate profiles

- [1] R. L. White, E. M. M. John, J. E. Baldwin, E. P. Abraham, *Biochem. J.* **1982**, *203*, 791.
- [2] B. O. Bachmann, R. Li, C. A. Townsend, *Proc. Natl. Acad. Sci. USA* **1998**, *95*, 9082.
- [3] H. J. McNaughton, J. E. Thirkettle, Z. Zhang, C. J. Schofield, S. E. Jensen, B. Barton, P. Greaves, *Chem. Commun.* **1998**, 2325.
- [4] L. E. Nunez, C. Mendez, A. F. Brana, G. Blanco, J. A. Salas, *Chem. Biol.* **2003**, *10*, 301.
- [5] M. F. Freeman, K. A. Moshos, M. J. Bodner, R. Li, C. A. Townsend, *Proc. Natl. Acad. Sci. USA* **2008**, *105*, 11128.
- [6] B. Gerratana, S. O. Arnett, A. Stapon, C. A. Townsend, *Biochemistry* **2004**, *43*, 15936.
- [7] R. F. Li, A. Stapon, J. T. Blanchfield, C. A. Townsend, *J. Am. Chem. Soc.* **2000**, *122*, 9296.
- [8] N. Khaleeli, R. F. Li, C. A. Townsend, *J. Am. Chem. Soc.* **1999**, *121*, 9223.
- [9] M. Merski, C. A. Townsend, *J. Am. Chem. Soc.* **2007**, *129*, 15750.
- [10] M. E. Caines, J. L. Sorensen, C. J. Schofield, *Biochem. Biophys. Res. Commun.* **2009**, *385*, 512.
- [11] B. O. Bachmann, C. A. Townsend, *Biochemistry* **2000**, *39*, 11187.
- [12] B. Gerratana, A. Stapon, C. A. Townsend, *Biochemistry* **2003**, *42*, 7836.
- [13] S. O. Arnett, B. Gerratana, C. A. Townsend, *Biochemistry* **2007**, *46*, 9337.
- [14] M. L. Raber, M. F. Freeman, C. A. Townsend, *J. Biol. Chem.* **2009**, *284*, 207.
- [15] M. T. Miller, B. O. Bachmann, C. A. Townsend, A. C. Rosenzweig, *Proc. Natl. Acad. Sci. USA* **2002**, *99*, 14752.
- [16] M. T. Miller, B. O. Bachmann, C. A. Townsend, A. C. Rosenzweig, *Nat. Struct. Biol.* **2001**, *8*, 684.
- [17] M. L. Raber, S. O. Arnett, C. A. Townsend, *Biochemistry* **2009**, *48*, 4959.
- [18] J. M. Fox, O. Dmitrenko, L. A. Liao, R. D. Bach, *J. Org. Chem.* **2004**, *69*, 7317.
- [19] A. C. Hengge, R. A. Hess, *J. Am. Chem. Soc.* **1994**, *116*, 11256.
- [20] W. P. Jencks, *Acc. Chem. Res.* **1980**, *13*, 161.
- [21] D. Stefanidis, S. Cho, S. Dhepaganon, W. P. Jencks, *J. Am. Chem. Soc.* **1993**, *115*, 1650.
- [22] D. Stefanidis, W. P. Jencks, *J. Am. Chem. Soc.* **1993**, *115*, 6045.
- [23] T. T. Tidwell, *Angew. Chem.* **2005**, *117*, 5926; *Angew. Chem. Int. Ed.* **2005**, *44*, 5778.
- [24] W. E. Truce, P. S. Bailey, *J. Org. Chem.* **1969**, *34*, 1341.
- [25] B. S. Gerstenberger, J. Lin, Y. S. Mimieux, L. E. Brown, A. G. Oliver, J. P. Kopolinski, *Org. Lett.* **2008**, *10*, 369.
- [26] S. Ba-Saif, A. K. Luthra, A. Williams, *J. Am. Chem. Soc.* **1987**, *109*, 6362.
- [27] S. Ba-Saif, A. K. Luthra, A. Williams, *J. Am. Chem. Soc.* **1989**, *111*, 2647.
- [28] A. Williams, K. T. Douglas, *Chem. Rev.* **1975**, *75*, 627.
- [29] S. A. Deraniyagala, S. A. Adediran, R. F. Pratt, *J. Org. Chem.* **1995**, *60*, 1619.
- [30] M. I. Page, *J. Am. Chem. Soc.* **1984**, *106*, 144.
- [31] T. Simonson, *Curr. Opin. Struct. Biol.* **2001**, *11*, 243.
- [32] T. Simonson, C. L. Brooks, *J. Am. Chem. Soc.* **1996**, *118*, 8452.
- [33] Y. V. Guillen Schlippe, L. Hedstrom, *Arch. Biochem. Biophys.* **2005**, *433*, 266.
- [34] K. L. Rebholz, D. B. Northrop, *Methods Enzymol.* **1995**, *249*, 211.
- [35] K. L. Rebholz, D. B. Northrop, *Biochem. Biophys. Res. Commun.* **1991**, *176*, 65.
- [36] L. Toulkhonova, W. J. Metzler, M. R. Witmer, R. A. Copeland, J. Marcinkiewicz, *J. Biol. Chem.* **2003**, *278*, 4582.
- [37] L. J. Hyland, T. A. Tomaszek, Jr., T. D. Meek, *Biochemistry* **1991**, *30*, 8454.
- [38] R. T. Raines, J. R. Knowles, *Biochemistry* **1987**, *26*, 7014.
- [39] S. Rozovsky, A. E. McDermott, *Proc. Natl. Acad. Sci. USA* **2007**, *104*, 2080.
- [40] A. C. Brouwer, J. F. Kirsch, *Biochemistry* **1982**, *21*, 1302.
- [41] A. E. Reed, L. A. Curtiss, F. Weinhold, *Chem. Rev.* **1988**, *88*, 899.
- [42] C. A. Townsend, *Curr. Opin. Chem. Biol.* **2002**, *6*, 583.
- [43] N. J. Kershaw, M. E. Caines, M. C. Sleeman, C. J. Schofield, *Chem. Commun.* **2005**, 4251.
- [44] S. Derzelle, E. Duchaud, F. Kunst, A. Danchin, P. Bertin, *Appl. Environ. Microbiol.* **2002**, *68*, 3780.
- [45] T. G. Kinscherf, D. K. Willis, *J. Antibiot.* **2005**, *58*, 817.
- [46] M. D. Lloyd, K. D. Merritt, V. Lee, T. J. Sewell, B. Wha-Son, J. E. Baldwin, C. J. Schofield, S. W. Elson, K. H. Baggaley, N. H. Nicholson, *Tetrahedron* **1999**, *55*, 10201.
- [47] M. J. Frisch et al., Gaussian, Inc., revision B.05, Pittsburgh, PA, **2003**.
- [48] C. J. Cramer, *Essentials of Computational Chemistry: Theory and Models*, 2nd ed., Wiley, New York, **2004**.
- [49] K. N. Houk, P. H. Y. Cheong, *Nature* **2008**, *455*, 309.
- [50] F. Jensen, *Introduction to Computational Chemistry*, 2nd ed., Wiley, Chichester, UK, **2007**.
- [51] P. R. Schreiner, A. A. Fokin, R. A. Pascal, A. de Meijere, *Org. Lett.* **2006**, *8*, 3635.
- [52] M. D. Wodrich, C. Corminboeuf, P. R. Schreiner, A. A. Fokin, P. V. Schleyer, *Org. Lett.* **2007**, *9*, 1851.
- [53] Y. Zhao, D. G. Truhlar, *Org. Lett.* **2006**, *8*, 5753.
- [54] Y. Zhao, N. Gonzalez-Garcia, D. G. Truhlar, *J. Phys. Chem. A* **2005**, *109*, 2012.
- [55] Y. Zhao, D. G. Truhlar, *Acc. Chem. Res.* **2008**, *41*, 157.
- [56] T. Borowski, E. Broclawik, C. J. Schofield, P. E. M. Siegbahn, *J. Comput. Chem.* **2006**, *27*, 740.
- [57] I. Fernandez, M. A. Sierra, M. J. Mancheno, M. Gomez-Gallego, F. P. Cossio, *J. Am. Chem. Soc.* **2008**, *130*, 13892.
- [58] R. Lopez, M. I. Menendez, N. Diaz, D. Suarez, P. Campomanes, D. Ardura, T. L. Sordo, *Curr. Org. Chem.* **2006**, *10*, 805.
- [59] A. Macias, A. M. Ramallal, E. Alonso, C. del Pozo, J. Gonzalez, *J. Org. Chem.* **2006**, *71*, 7721.
- [60] H. Park, E. N. Brothers, K. M. Merz, *J. Am. Chem. Soc.* **2005**, *127*, 4232.



- [61] P. Perez-Faginas, I. A. M. T. Garcia-Lopez, R. Gonzalez-Muniz, *Tetrahedron Lett.* **2008**, *49*, 215.
- [62] K. W. Wiitala, Z. X. Tian, C. J. Cramer, T. R. Hoye, *J. Org. Chem.* **2008**, *73*, 3024.
- [63] D. Xu, H. Guo, G. Cui, *J. Am. Chem. Soc.* **2007**, *129*, 10814.
- [64] R. Dennington II, T. Keith, J. Millam, K. Eppinnett, W. L. Hovell, R. Gilliland, GaussView, Version 3.09; Semichem, Inc.: Shawnee Mission, KS, 2003.

---

Received: June 25, 2009  
Published online on October 30, 2009